
PET Imaging of Serotonin Transporters with [¹¹C]DASB: Test–Retest Reproducibility Using a Multilinear Reference Tissue Parametric Imaging Method

Jae Seung Kim, MD^{1,2}; Masanori Ichise, MD^{1,3}; Janet Sangare, MS¹; and Robert B. Innis, MD, PhD¹

¹Molecular Imaging Branch, National Institute of Mental Health, Bethesda, Maryland; ²Department of Nuclear Medicine, Asan Medical Center, University of Ulsan College of Medicine, Seoul, Korea; and ³Nuclear Medicine Division, Brain Molecular Imaging Program, Brigham and Women's Hospital, Harvard Medical School, Boston, Massachusetts

Parametric imaging of serotonin transporters (SERT) with ¹¹C-labeled 3-amino-4-(2-dimethylaminomethyl-phenylsulfanyl)-benzonitrile ([¹¹C]DASB) PET is a useful data analysis tool. The purpose of this study was to evaluate the reproducibility of measurements of SERT binding potential (*BP*) and relative blood flow (*R*₁) by a 2-parameter multilinear reference tissue parametric imaging method (MRTM2) for human [¹¹C]DASB studies.

Methods: Eight healthy subjects (3 men, 5 women; age, 26 ± 9 y) underwent 2 [¹¹C]DASB PET scans separated by 1 h on the same day (dose, 703 ± 111 MBq). Parametric images of *BP* and *R*₁ were generated by MRTM2 using the cerebellum as a reference region. The *k*₂ (clearance rate constant from the reference region) required by MRTM2 was estimated by the 3-parameter MRTM. Reproducibility of *BP* and *R*₁ measurements was evaluated by calculating bias (100 × (retest – test)/test), variability (SD of the bias), and reliability (intraclass correlation coefficient = ρ) for several representative regions of interest (ROIs). *BP* and *R*₁ were estimated for ROI time–activity curves fitted by MRTM2 and were compared with those based on the parametric images. **Results:** The test–retest (0.066 ± 0.013/0.06 ± 0.011 min⁻¹) MRTM *k*₂ reproducibility was excellent with small bias (3%) and variability (6%) and high reliability (0.95). Retest *BP* values were consistently lower than those of test *BP* values in all regions (a mean negative bias of ~6%; *P* < 0.001). The test–retest *BP* variability was relatively small, ranging from 4% to 13%, with ρ ranging from 0.44 to 0.85. In contrast to *BP*, test–retest *R*₁ values were similar with negligible bias of ≤0.1%. The test–retest *R*₁ variability was excellent and smaller than that of *BP* ranging from 3% to 6%, with ρ ranging from 0.58 to 0.95. *BP* and *R*₁ values estimated by the ROI time–activity curve-fitting method were slightly lower (~3% and ~1%, respectively) than those by the parametric imaging method (*P* < 0.001). However, the test–retest bias and variability of *BP* and *R*₁ were very similar for both ROI and parametric methods. **Conclusion:** Our results suggest that [¹¹C]DASB parametric

imaging of *BP* and *R*₁ with the noninvasive MRTM2 method is reproducible and reliable for PET studies of SERT.

Key Words: PET; parametric imaging; reproducibility; linearized reference tissue model; [¹¹C]DASB; serotonin transporters; non-invasive quantification

J Nucl Med 2006; 47:208–214

The serotonin transporter (SERT) is located on the cell body and presynaptic terminals of the serotonergic neuron and plays an important role in the regulation of serotonergic neurotransmissions by means of reuptake of released serotonin in the synaptic cleft. Abnormalities of SERT have been described in several neuropsychiatric conditions, such as depression and obsessive–compulsive disorder (1–9). Therefore, in vivo imaging of the SERT has been of interest as a tool to study serotonin function in health and disease. A recently developed highly selective radioligand, ¹¹C-labeled 3-amino-4-(2-dimethylaminomethyl-phenylsulfanyl)-benzonitrile ([¹¹C]DASB), has been successfully used for PET imaging of SERT in human brain (10–14). The estimated radiation burden of [¹¹C]DASB is relatively small and would allow multiple PET examinations of the same research subject per year (15).

[¹¹C]DASB tissue data can be described by a 1-tissue (1T) compartment model (10), and SERT binding potential (*BP*) (16), which correlates well with SERT densities (10,11), can be estimated using the cerebellum, which contains few SERT-binding sites, as reference tissue. Reference tissue methods have been widely used to estimate neuroreceptor *BP* because these methods eliminate the invasive and often logistically difficult procedure of obtaining arterial input functions corrected for metabolites.

A computationally fast and noise-resistant parameter estimation method, called 2-parameter linearized reference tissue model (MRTM2), allows parametric imaging of *BP*

Received May 29, 2005; revision accepted Nov. 2, 2005.

For correspondence or reprints contact: Jae Seung Kim, MD, Department of Nuclear Medicine, Asan Medical Center, 388-1 Poongnap-dong, Songpa-gu, Seoul, 138-736 Korea.

E-mail: jaeskim@amc.seoul.kr

and relative tracer delivery (R_1) from dynamic [^{11}C]DASB PET data (17). In the present study, we evaluated the reproducibility of voxel-based measurements of SERT BP and R_1 by MRTM2 in healthy volunteers, as the demonstration of a reproducible PET outcome measure is critical and preliminary to the extension of [^{11}C]DASB PET to clinical populations such as depression and obsessive-compulsive disorders.

MATERIALS AND METHODS

Subjects

The study was conducted under the approval of the Institutional Review Board of the National Institute of Mental Health. Three male and 5 female healthy volunteers (mean age, 26 ± 9 y; age range, 19–41 y) participated in the study after providing written informed consent. All subjects were free of medical or neuropsychiatric illness on the basis of a screening assessment consisting of history, physical examination, routine blood and urine tests, and electrocardiography.

Radiopharmaceutical Preparation

[^{11}C]DASB was synthesized as previously described (18) by ^{11}C -methyl iodide reaction with the corresponding desmethyl precursor. The radiochemical purities of syntheses used for the study were $96.0\% \pm 2.9\%$, with corresponding specific activities of 49.6 ± 10.4 GBq/ μmol (1.34 ± 0.28 Ci/ μmol) at the time of injection. These and subsequent data are expressed as mean \pm SD.

PET Data Acquisition

All subjects underwent a [^{11}C]DASB PET scan (test) and a repeated PET scan (retest) separated by 1 h on the same day. Subjects were placed on the scanner bed with his or her head held firmly in place with a thermoplastic mask fixed to the bed to minimize head movement during each scan. After an 8-min transmission scan using a ^{68}Ge rotating pin source, dynamic PET scans were acquired on the Advance tomograph (GE Healthcare) in the 3-dimensional mode for 120 min (33 successive frames consisting of 6×0.5 , 3×1 , 2×2 , and 22×5 min frames) after bolus administration of 703 ± 111 MBq of [^{11}C]DASB. The GE Advance acquires 35 simultaneous slices, with 4.25-mm interslice distance with a reconstructed spatial resolution of 6 mm in all directions.

To be used for image coregistration and anatomic reference, all subjects also had T1-weighted MRI (repetition time/echo time = 14/5.4), acquired on a 1.5-T Horizon scanner (GE Healthcare)

MRTM2

The operational equation for the MRTM2 (17) is:

$$C(T) = R_1 \left(k'_2 \int_0^T C'(t) dt + C'(T) \right) - k_2 \int_0^T C(T) dt, \quad \text{Eq. 1}$$

where $C(T)$ and $C'(T)$ are the region of interest (ROI) or voxel tissue tracer concentrations, k_2 and k'_2 are the tracer clearance rate constants from tissue, R_1 is the relative tracer delivery (K_1/K'_1), and the prime sign indicates the reference region. Equation 1 is applicable to the entire time–activity data for [^{11}C]DASB with 1T compartment model kinetics—that is, for $T > 0$. MRTM2 allows estimation of BP = $(R_1 k'_2 / k_2 - 1)$ and R_1 using a receptor-free reference region (cerebellum). When given a priori the correct

value of k'_2 , the MRTM2 parameter estimation is nearly identical to that of nonlinear 1T kinetic analysis (1TKA) (19) but MRTM2 parameter estimation can be performed in a fraction of the computational time required for the nonlinear version of MRTM2 (17). The value of k'_2 can be estimated by the 3-parameter MRTM using ROI time–activity curves. The operational equation of MRTM is:

$$C(T) = R_1 k'_2 \int_0^T C'(t) dt - k_2 \int_0^T C(t) dt + R_1 C'(T). \quad \text{Eq. 2}$$

Equation 2 estimates 3 parameters, R_1 , k'_2 , and k_2 , using the reference and target tissue time–activity curves. Because a different value of k'_2 is estimated by Equation 2 for each ROI time–activity curve, although there is only 1 reference region and, therefore, only 1 true value for k'_2 , a 2-parameter version (MRTM2) of Equation 2 is obtained by fixing k'_2 to a value obtained with a preliminary analysis using Equation 2.

Parametric Imaging

The original reconstructed PET data were corrected for subject motion by registering each frame to a summed image of all frames in the statistical parametric software, SPM2 (Wellcome Department of Cognitive Neurology, London, U.K.). Our previous computer data simulation analysis showed that parametric images of R_1 generated by MRTM2 are accurate even when incorrect values of k'_2 are used and the statistical quality of the parametric images is nearly identical to those estimated by 1TKA (20). Although R_1 images may not be of primary interest for [^{11}C]DASB, these images reflect relative blood flow and are useful for brain structure identification and image coregistration with MRI. In the present study, we took advantage of this property of R_1 images to do parametric imaging in 2 steps. First, preliminary R_1 images were generated with a k'_2 value estimated by MRTM. Two ROIs for the cerebellum and thalamus were manually defined on the summed motion-corrected dynamic PET images, and k'_2 was estimated with these 2 time–activity curves using MRTM and used to generate preliminary R_1 images by MRTM2 with the cerebellum as a reference region. All MRTM (Eq. 2) and MRTM2 (Eq. 1) linear least-squares fitting was done with scan data weighted by $(1/\text{SD}^2)$, where SD of the data was estimated based on the noise-equivalent counts as described previously (21). Parametric images were generated with the pixelwise modeling software PMOD 2.5 (PMOD group) (22), installed on a personal computer workstation (Dell Computer Co., 1.7-GHz Pentium IV/1-GB RAM running Windows 2000, Microsoft Co.).

In the second step, the subject's MR images were coregistered to the preliminary R_1 images in SPM2. Then, these 2 image sets were fused using an image fusion tool in PMOD. Several anatomic ROIs were manually defined on these fused images. These ROIs were placed on the motion-corrected dynamic data to obtain ROI time–activity curves from the cerebellum ($1,131 \pm 188$ voxels; voxel size, $6.0 \times 6.0 \times 4.25$ mm), raphe (87 ± 6 voxels), striatum (220 ± 73 voxels), thalamus (228 ± 90 voxels), frontal cortex (386 ± 52 voxels), temporal cortex ($1,621 \pm 331$ voxels), and occipital cortex ($1,578 \pm 286$ voxels). To minimize the variability of k'_2 estimation by MRTM, a weighted (according to ROI size) mean k'_2 value over raphe, thalamus, and striatum with the cerebellum as a reference region was used for parametric imaging of BP and R_1 by MRTM2 (17).

For the retest data, preliminary R_1 parametric images were generated as for the test data. Then, these preliminary R_1 images of the retest study were coregistered to the R_1 images of the test study. The alignment matrix generated to align the 2 R_1 parametric images was then applied to the individual frames of the second (retest) dynamic PET scan. The MRTM2 parametric images of BP and R_1 for the retest PET study were then generated as above except that the same ROIs defined for the test study were applied in the retest study.

After generation of MRTM2 parametric images of BP and R_1 , we obtained BP and R_1 values of the test and retest study for the raphe, thalamus, striatum, frontal cortex, temporal cortex, and occipital cortex with the same ROIs defined for the test study. Finally, BP and R_1 values were also estimated from the ROI time-activity curve data fitted by MRTM2, in contrast to voxelwise fitting in the parametric imaging.

Reproducibility Analysis

For parametric image-based BP and R_1 measurements as well as those ROI time-activity curve-based measurements, the test-retest reproducibility was evaluated by calculating bias, variability, and reliability (intraclass correlation coefficient (ICC)). The test-retest bias was calculated as the difference between the 2 measurements, expressed as a percentage of the value of the first measurement ($100 \times (\text{retest} - \text{test}/\text{test})$). The test-retest variability was calculated as the SD of the bias. The test-retest reliability of the 2 SERT binding parameter measurements was the ICC calculated according to the following equation (23):

$$\rho = \frac{MSBS - MSWS}{MSBS + (k - 1)MSWS}, \quad \text{Eq. 3}$$

where MSBS and MSWS are the mean sum of squares between and within subjects, respectively, and k is the number of within-subject measurements, being 2 in the present study. This coefficient is an estimate of the reliability of the 2 sets of measurements and varies from 0 (no reliability) to 1 (total reliability). Comparison between MRTM2 parametric imaging method and ROI time-activity curve methods was made with Wilcoxon matched pairs test. Statistical significance was defined as $P < 0.05$. All statistical analyses were performed in STATISTICA (StatSoft, Inc.).

For voxel-by-voxel comparison between the test and retest studies, BP and R_1 parametric images were spatially normalized to MNI T1 MR template provided by SPM2 using a coregistered T1 MR image of each subject. Subsequently, these images were smoothed with an isotropic gaussian filter to a final resolution of 12-mm full width at half maximum. Voxelwise comparison of BP and R_1 between the test and retest studies was performed using SPM2, assuming a cutoff level of $P < 0.05$ (height threshold) and an extent threshold of 100 voxels.

RESULTS

The test-retest k_2' values estimated by MRTM are summarized in Table 1. There was no significant difference in mean k_2' values between test and retest. The test-retest k_2' bias (3%) and variability (6%) were both small, and the reliability (0.95) was excellent. [^{11}C]DASB SERT BP was high in the raphe and hypothalamus, moderate in the thalamus and striatum, low in the cingulate gyrus, and absent in the cerebellum. Figure 1 shows test-retest parametric images of BP and R_1 of a representative subject and illustrates excellent reproducibility of regional distribution of BP and R_1 in the raphe, thalamus, and cingulate gyri.

The test-retest results of regional BP and R_1 estimated by MRTM2 parametric imaging method are summarized in Tables 2 and 3, respectively. Retest BP values were consistently lower than those of test values in all regions (a mean negative bias of $\sim 6\%$; $P < 0.001$). The test-retest BP variability was relatively small, ranging from 4% to 13%. High specific binding regions, including raphe, thalamus, and striatum, showed lower variability ($\sim 5\%$) than low specific binding regions, including frontal, temporal, and occipital cortex ($\sim 11\%$). The test-retest BP reliability (ICC, ρ) was moderate to high, ranging from 0.44 to 0.85 (Table 2).

In contrast to BP , R_1 values of all ROIs were not significantly different between test and retest ($P = 0.843$). The mean test-retest R_1 bias across all ROIs was trivial ($< 0.1\%$). The test-retest R_1 variability ($\sim 5\%$) was excellent and ranged from 3% to 6%. The test-retest R_1 reliability ranged from 0.58 to 0.95 and was slightly higher than that of BP

TABLE 1
Summary of Test and Retest k_2' Estimation

Subject no.	Age (y)	Sex	k_2' (min^{-1})*		% difference
			Test	Retest	
1	41	M	0.049	0.052	6.6
2	41	F	0.067	0.073	9.5
3	21	M	0.066	0.066	-0.1
4	20	M	0.055	0.058	5.4
5	22	F	0.082	0.076	-7.1
6	24	F	0.079	0.077	-3.0
7	23	F	0.079	0.079	-0.6
8	19	F	0.051	0.056	9.7
Mean \pm SD	26 \pm 9		0.066 \pm 0.013	0.067 \pm 0.011	2.5 \pm 6.2

*Mean k_2' value estimated with MRTM model on thalamus, striatum, and raphe time-activity curve with cerebellum as a reference region.

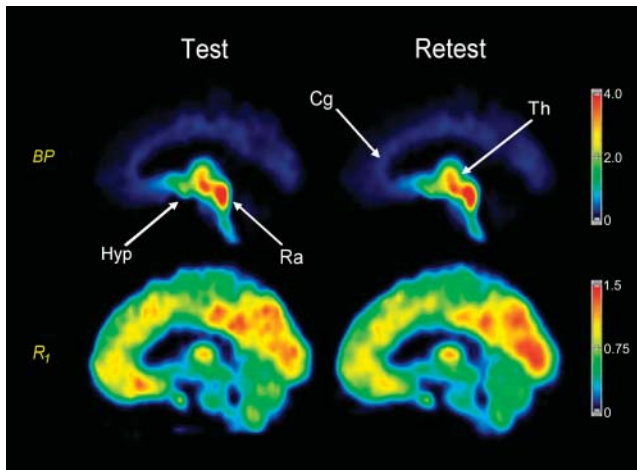


FIGURE 1. Test (left column) and retest (right column) parametric images of BP (top row) and R_1 (bottom row) of a representative subject. Th = thalamus; Ra = raphe; Hyp = hypothalamus; Cg = cingulate gyrus.

(Table 3). Thus, the MRTM2 parametric imaging method showed excellent test–retest reproducibility of BP and R_1 , although there was a small negative bias for BP measurements and R_1 reproducibility was overall slightly better than that of BP .

SPM comparison of BP and R_1 images obtained by the test and retest studies using a height threshold of uncorrected $P = 0.05$ and an extent threshold of 100 voxels showed a decrease of BP values in the retest study in the hypothalamus, thalamus, striatum, raphe, left midtemporal gyrus, and anterior cingulate gyrus but no significant differences for R_1 values (Fig. 2).

The test–retest results of BP and R_1 estimated by the ROI time–activity curve–fitting method by MRTM2 are summarized Tables 4 and 5, respectively. BP and R_1 values estimated by the ROI time–activity curve–fitting method by MRTM2 were slightly lower ($\sim 3\%$ and $\sim 1\%$, respectively) than those estimated by the MRTM2 parametric imaging method ($P < 0.001$). However, the test–retest bias and variability of BP and R_1 were similar for the 2 methods.

DISCUSSION

We evaluated the test–retest reproducibility of [^{11}C]DASB PET measurements of SERT BP and R_1 in healthy volunteers

using a computationally fast and noise-resistant parameter estimation method, MRTM2. The MRTM2 parametric imaging method showed excellent test–retest reproducibility of BP and R_1 measurements, with variability ranging from 3% to 13%, but with a small negative bias (6%) for BP measurements. This demonstration of a reproducible PET outcome measure is critical and preliminary to the extension of [^{11}C]DASB PET to clinical populations, such as depression and obsessive–compulsive disorders.

The MRTM2 parameter estimation requires a priori MRTM k'_2 estimation using ROI time–activity curves. The test–retest reproducibility of MRTM k'_2 estimation was excellent, where we used ROI size–weighted mean k'_2 values over raphe, thalamus, and striatum with the cerebellum as a reference region. The k'_2 variability of 6% in the present study was the same as that of our previous computer data simulation analysis (17).

In the present study, the test–retest variability of BP (ranging from 4% to 13%) and R_1 (ranging from 3% to 6%) measurements by the MRTM2 parametric imaging method was excellent and generally consistent with the results of our previous simulation analysis with 5%–10% noise (17). Previously the variability of raphe BP estimation was significantly higher than that of the striatum, probably because of the shorter scanning duration used in the prior study (90 vs. 120 min). However, with the current 120-min scanning, the variability of raphe BP (7%) was only marginally higher than that of striatum (5%). With the short half-life of ^{11}C (20.4 min), however, scanning up to 120 min results in higher statistical noise in the latter part of the data. To improve parameter estimations, therefore, in the current study we applied weighted least-squares estimations to account for noise-level differences in $C(T)$ (24). The scan duration is an important factor to consider when evaluating a prospective new PET radioligand for human study. The scan duration needs to be long enough to obtain stable estimates of receptor-related parameters but short enough both to meet subject compliance and to avoid excessive distortion of the time–activity data by incremental noise (10,25). For [^{11}C]DASB, lengthening of the scan duration from 90 to 120 min appears instrumental to improve parameter estimation at the voxel level for regions with high BP , such as the raphe, although Ginovart et al. (10) showed

TABLE 2
Test–Retest Bias, Variability, and Reliability of BP Estimated by MRTM2 Parametric Imaging Method

Region	BP (mean \pm SD; $n = 8$)		Bias (%)	Variability (%)	Reliability (ρ)
	Test	Retest			
Striatum	1.38 \pm 0.18	1.31 \pm 0.14	–4.8	4.5	0.83
Thalamus	2.10 \pm 0.34	1.94 \pm 0.31	–7.5	4.1	0.85
Raphe	3.24 \pm 0.27	3.00 \pm 0.20	–7.0	4.8	0.45
Frontal cortex	0.41 \pm 0.05	0.38 \pm 0.03	–6.9	8.7	0.44
Temporal cortex	0.58 \pm 0.13	0.56 \pm 0.11	–2.5	8.9	0.85
Occipital cortex	0.39 \pm 0.11	0.37 \pm 0.08	–4.3	12.8	0.83

TABLE 3
Test–Retest Bias, Variability, and Reliability of R_1 Estimated by MRTM2 Parametric Imaging Method

Region	R_1 (mean \pm SD; $n = 8$)		Bias (%)	Variability (%)	Reliability (ρ)
	Test	Retest			
Striatum	1.03 \pm 0.07	1.02 \pm 0.07	−0.9	2.5	0.92
Thalamus	1.03 \pm 0.08	1.02 \pm 0.06	−0.8	6.1	0.62
Raphe	0.77 \pm 0.08	0.76 \pm 0.05	−0.9	5.7	0.73
Frontal cortex	0.97 \pm 0.11	0.97 \pm 0.11	−0.6	3.5	0.95
Temporal cortex	0.71 \pm 0.05	0.71 \pm 0.07	0.0	4.3	0.87
Occipital cortex	1.00 \pm 0.06	1.03 \pm 0.08	3.0	6.4	0.58

that a 90-min study is probably adequate for ROI-based [^{11}C]DASB analyses.

In the current study, the retest BP was lower by 6% across all regions but R_1 did not differ between test and retest. Most reproducibility studies of neuroreceptor imaging show no significant systematic differences in BP between test and retest scans. However, in contrast to our current study, in the studies reporting no systematic parameter estimation bias, test and retest scans were performed on separate days (26–28). We do not know the cause of the consistently lower BP values on retest compared with test scans, but it may have been the effect of residual carrier from the first scan, diurnal variation, or even the stress from the scanning procedure. As a worst-case scenario, the occupancy of SERT by residual carrier from the first injection can be estimated from the occupancy at time of peak uptake in the thalamus during the test scan. At the time of peak specific binding uptake in the thalamus (~80 min after injection), the average specific binding concentration of tracer in thalamus was 0.8 ± 0.3 nmol/L. The density of SERT (maximum number of binding sites [B_{max}]) in human thalamus has been estimated to be 12–24 nmol/L (29,30). Thus, at the time of maximal brain uptake, [^{11}C]DASB is estimated to occupy 3%–6% of all SERT. In addition, by the time of the retest scan, about half of the carrier would have washed out of the brain. Thus, residual carrier would have caused only a minimal component of the 6% negative bias. Other possible causes include a diurnal variation in SERT levels (since the test

scan was always in the morning and the retest in the afternoon) (31,32) or possibly the effect of stress of participating in the first scan. Acute stress activates a series of physiologic systems as part of the adaptive response that is characterized by elevation of circulating cortisol and modulation of serotonergic neuronal activity (33,34). Tafet et al. reported that the elevated cortisol induced by stress increases serotonin uptake owing to promotion of synthesis of the SERT (35). However, we do not know the relationship between the regional change of serotonergic neuron and the quality of acute stress. Further investigation with [^{11}C]DASB PET may be interesting in this regard.

The ICC is a measure of the correlation between the values obtained with 2 methods within the same subject (23). It has been used as an index of the reliability of test–retest measurements (26,36–39). The ICC combines information on the systemic difference between methods (test and retest) and that of the random measurement variation. As apparent from Equation 3, given the same test–retest variability (MSWS), the ICC of a measure with a large intersubject variability (MSBS) will be higher than that of a measure with a small intersubject variability. For example, the ICC for raphe was only moderate (0.5) in the raphe, despite the small test–retest variability of 5%. This ICC value of only 0.5 is caused by the small intersubject BP variability (coefficient of variation = $100 \times \text{SD}/\text{mean}$) of 8% for raphe as opposed to the large intersubject BP variability of 28% for occipital cortex, for example, where the ICC was 0.8 and the test–retest variability was 13% (Table 2).

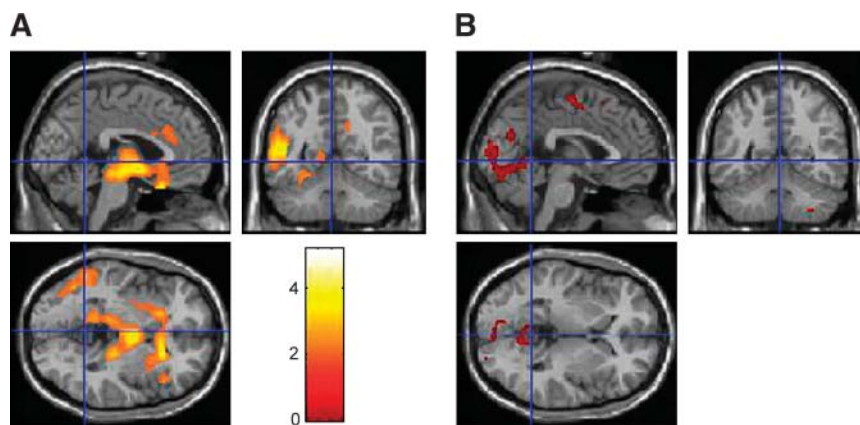


FIGURE 2. MRI superimposed with t -statistic maps obtained from SPM comparing test and retest studies using height threshold of uncorrected $P = 0.05$ and extent threshold of 100 voxels. (A) t -statistic maps comparing BP values of test and retest (test $>$ retest). (B) t -statistic maps comparing R_1 values of test and retest (test $<$ retest).

TABLE 4
Test–Retest Bias, Variability, and Reliability of *BP* Estimated by ROI Time–Activity Curve-Fitting Method

Region	<i>BP</i> (mean ± SD; <i>n</i> = 8)		Bias (%)	Variability (%)	Reliability (ρ)
	Test	Retest			
Striatum	1.38 ± 0.19	1.32 ± 0.16	−4.3	3.7	0.89
Thalamus	2.04 ± 0.34	1.88 ± 0.30	−7.5	4.6	0.84
Raphe	3.16 ± 0.26	2.93 ± 0.19	−7.0	5.3	0.39
Frontal cortex	0.40 ± 0.06	0.37 ± 0.03	−6.8	8.0	0.55
Temporal cortex	0.53 ± 0.13	0.51 ± 0.10	−2.7	9.7	0.82
Occipital cortex	0.39 ± 0.12	0.36 ± 0.09	−4.5	13.2	0.85

Frankle et al. reported, in an abstract, the test–retest variability and ICC of *BP* measured with [¹¹C]DASB using ROI but not parametric images (39). These authors obtained an arterial input function and used a constrained 2-tissue compartment model with nonlinear fitting. The test–retest variability of *BP* (10% for central regions and 25% for neocortical regions) was higher, but the test–retest reliability of *BP* (ICC, 0.94~0.97) was better than that of our present study. The mean injected dose of radiopharmaceutical (518 MBq) was lower than ours (703 MBq). In addition to differences in analytic method, different ROI sizes may have caused differences in the variability and reliability. In any case, parametric analysis has several advantages over the ROI approach, including the use of SPM to identify alterations in receptor binding in all areas of the brain in 2 groups of subjects.

In the present study, *BP* and *R*₁ values estimated by the ROI time–activity curve-fitting method were slightly lower than those by the parametric imaging method. Nevertheless, both methods showed equally excellent reproducibility of *BP* and *R*₁ measurements. Here, the difference between the 2 methods relates to the difference in data noise at the time of fitting. In parametric imaging, MRTM2 fitting is done at a voxel noise level, whereas in ROI time–activity curve estimation, MRTM2 fitting is done at a ROI noise level. Therefore, individual voxel *BP* or *R*₁ estimations will have a larger variability than that of ROI *BP* or *R*₁ estimations. However, the results of the present study show that *BP* or *R*₁ estimations by MRTM2 parametric imaging for a ROI obtained by averaging voxel *BP* or *R*₁ values within the

ROI have the same robustness as those obtained by MRTM2 fitting of the ROI time–activity curve.

Finally, we did not perform invasive 1TKA *BP* and *R*₁ estimations in the present study. In our prior publication, MRTM2 *BP* and *R*₁ estimations were very close to those of 1TKA that required metabolite-corrected arterial input functions (17). However, MRTM2 estimations were not identical to those of 1TKA, with opposing effects. First, MRTM2 requires a priori *k*₂ estimation by MRTM. The inaccuracy of *k*₂ estimation, therefore, can increase the variability of MRTM2 estimations. Second, 1TKA estimation requires metabolite-corrected arterial plasma data. Therefore, any error in blood data could increase the variability of 1TKA estimations. Thus, the only way to evaluate which method—noninvasive MRTM2 or invasive 1TKA—is more reproducible would have been to include the 1TKA method in the present study design.

CONCLUSION

Our results suggest that [¹¹C]DASB parametric imaging of *BP* and *R*₁ by noninvasive MRTM2 and without arterial sampling is a reproducible and reliable method for PET of SERT.

ACKNOWLEDGMENTS

We gratefully acknowledge the NIH Clinical Center radiochemistry staff (directed by Michael Channing, PhD) and imaging staff (directed by Peter Herscovitch, MD) for the successful completion of this study.

TABLE 5
Test–Retest Bias, Variability, and Reliability of *R*₁ Estimated by ROI Time–Activity Curve-Fitting Method

Region	<i>R</i> ₁ (mean ± SD; <i>n</i> = 8)		Bias (%)	Variability (%)	Reliability (ρ)
	Test	Retest			
Striatum	1.03 ± 0.07	1.02 ± 0.07	−1.1	2.9	0.89
Thalamus	1.03 ± 0.08	1.01 ± 0.06	−1.0	6.3	0.55
Raphe	0.77 ± 0.08	0.76 ± 0.04	−1.0	6.3	0.67
Frontal cortex	0.96 ± 0.11	0.96 ± 0.11	−0.7	3.2	0.96
Temporal cortex	0.69 ± 0.05	0.69 ± 0.06	0.0	4.6	0.85
Occipital cortex	1.00 ± 0.07	1.02 ± 0.08	2.8	6.5	0.60

REFERENCES

- Crow TJ, Cross AJ, Cooper SJ, et al. Neurotransmitter receptors and monoamine metabolites in the brains of patients with Alzheimer-type dementia and depression, and suicides. *Neuropharmacology*. 1984;23:1561–1569.
- Lopez-Ibor JJ Jr. The involvement of serotonin in psychiatric disorders and behaviour. *Br J Psychiatry Suppl*. 1988;Sep(3):26–39.
- Barr LC, Goodman WK, Price LH. The serotonin hypothesis of obsessive compulsive disorder. *Int Clin Psychopharmacol*. 1993;8(suppl 2):79–82.
- Leonard HL, Swedo SE, Rapoport JL, et al. Treatment of obsessive-compulsive disorder with clomipramine and desipramine in children and adolescents: a double-blind crossover comparison. *Arch Gen Psychiatry*. 1989;46:1088–1092.
- Goodman WK, McDougle CJ, Price LH. Pharmacotherapy of obsessive compulsive disorder. *J Clin Psychiatry*. 1992;53(suppl):29–37.
- Greist JH, Jefferson JW, Kobak KA, et al. Efficacy and tolerability of serotonin transport inhibitors in obsessive-compulsive disorder: a meta-analysis. *Arch Gen Psychiatry*. 1995;52:53–60.
- Weizman A, Carmi M, Hermesh H, et al. High-affinity imipramine binding and serotonin uptake in platelets of eight adolescent and ten adult obsessive-compulsive patients. *Am J Psychiatry*. 1986;143:335–339.
- Marazziti D, Hollander E, Lensi P, et al. Peripheral markers of serotonin and dopamine function in obsessive-compulsive disorder. *Psychiatry Res*. 1992;42:41–51.
- Bastani B, Arora RC, Meltzer HY. Serotonin uptake and imipramine binding in the blood platelets of obsessive-compulsive disorder patients. *Biol Psychiatry*. 1991;30:131–139.
- Ginovart N, Wilson AA, Meyer JH, et al. Positron emission tomography quantification of [¹¹C]DASB binding to the human serotonin transporter: modeling strategies. *J Cereb Blood Flow Metab*. 2001;21:1342–1353.
- Houle S, Ginovart N, Hussey D, et al. Imaging the serotonin transporter with positron emission tomography: initial human studies with [¹¹C]DAPP and [¹¹C]DASB. *Eur J Nucl Med*. 2000;27:1719–1722.
- Huang Y, Hwang D-R, Narendran R, et al. Comparative evaluation in nonhuman primates of five PET radiotracers for imaging the serotonin transporters: [¹¹C]McN 5652, [¹¹C]ADAM, [¹¹C]DASB, [¹¹C]DAPA, and [¹¹C]AFM. *J Cereb Blood Flow Metab*. 2002;22:1377–1398.
- Wilson AA, Ginovart N, Schmidt M, et al. Novel radiotracers for imaging the serotonin transporter by positron emission tomography: synthesis, radio-synthesis, and in vitro and ex vivo evaluation of ¹¹C-labeled 2-(phenylthio)-araalkylamines. *J Med Chem*. 2000;43:3103–3110.
- Meyer JH, Houle S, Sagrati S, et al. Brain serotonin transporter binding potential measured with carbon 11-labeled DASB positron emission tomography: effects of major depressive episodes and severity of dysfunctional attitudes. *Arch Gen Psychiatry*. 2004;61:1271–1279.
- Lu JQ, Ichise M, Liow JS, Ghose S, Vines D, Innis RB. Biodistribution and radiation dosimetry of the serotonin transporter ligand ¹¹C-DASB determined from human whole-body PET. *J Nucl Med*. 2004;45:1555–1559.
- Mintun MA, Raichle ME, Kilbourn MR, Wooten GF, Welch MJ. A quantitative model for the *in vivo* assessment of drug binding sites with positron emission tomography. *Ann Neurol*. 1984;15:217–227.
- Ichise M, Liow JS, Lu JQ, et al. Linearized reference tissue parametric imaging methods: application to [¹¹C]DASB positron emission tomography studies of the serotonin transporter in human brain. *J Cereb Blood Flow Metab*. 2003;23:1096–1112.
- Wilson AA, Ginovart N, Hussey D, et al. In vitro and in vivo characterisation of [¹¹C]DASB: a probe for in vivo measurements of the serotonin transporter by positron emission tomography. *Nucl Med Biol*. 2002;29:509–515.
- Wu Y, Carson RE. Noise reduction in the simplified reference tissue model for neuroreceptor functional imaging. *J Cereb Blood Flow Metab*. 2002;22:1440–1452.
- Ichise M, Cohen RM, Liow JS, et al. Estimation of normalized distribution volume without receptor-free reference region or arterial input function: application to the muscarinic-2 ligand [¹⁸F]FP-TZTP. *Neuroimage*. 2004;22(suppl 2):T149–T150.
- Carson RE, Kiesewetter DO, Jagoda E, et al. Muscarinic cholinergic receptor measurements with [¹⁸F]FP-TZTP: control and competition studies. *J Cereb Blood Flow Metab*. 1998;18:1130–1142.
- Burger C, Buck A. Requirements and implementation of a flexible kinetic modeling tool. *J Nucl Med*. 1997;38:1818–1823.
- Snedecor GW, Cochran WG. Specific indices of interater reliability. In: Snedecor GW, Cochran WG, eds. *Statistical Methods*. Ames, IA: Iowa State University Press; 1989:147–146.
- Carson RE. Parameter estimation in positron emission tomography. In: Phelps ME, Mazziotta JC, Schelbert HR, eds. *Positron Emission Tomography: Principles and Applications for the Brain and the Heart*. New York, NY: Raven Press; 1986:347–390.
- Laruelle M, Slifstein M, Huang Y. Relationships between radiotracer properties and image quality in molecular imaging of the brain with positron emission tomography. *Mol Imaging Biol*. 2003;5:363–375.
- Tsuchida T, Ballinger JR, Vines D, et al. Reproducibility of dopamine transporter density measured with ¹²³I-FPCIT SPECT in normal control and Parkinson's disease patients. *Ann Nucl Med*. 2004;18:609–616.
- Smith GS, Price JC, Lopresti BJ, et al. Test-retest variability of serotonin 5-HT_{2A} receptor binding measured with positron emission tomography and [¹⁸F]altanserin in the human brain. *Synapse*. 1998;30:380–392.
- Gage HD, Voytko ML, Ehrenkauf RL, et al. Reproducibility of repeated measures of cholinergic terminal density using [¹⁸F](+)-4-fluorobenzyltrozamicol and PET in the rhesus monkey brain. *J Nucl Med*. 2000;41:2069–2076.
- Plenge P, Mellerup ET, Laursen H. Regional distribution of the serotonin transport complex in human brain, identified with ³H-paroxetine, ³H-citalopram and ³H-imipramine. *Prog Neuropsychopharmacol Biol Psychiatry*. 1990;14:61–72.
- Rosel P, Menchon JM, Oros M, et al. Regional distribution of specific high affinity binding sites for ³H-imipramine and ³H-paroxetine in human brain. *J Neural Transm*. 1997;104:89–96.
- Meyerson LR, Strano R, Ocheret D. Diurnal concordance of human platelet serotonin content and plasma alpha-1-acid glycoprotein concentration. *Pharmacol Biochem Behav*. 1989;32:1043–1047.
- Martin KF. Rhythms in neurotransmitter turnover: focus on the serotonergic system. *Pharmacol Ther*. 1991;51:421–429.
- Bonnin A, Grimaldi B, Fillion MP, Fillion G. Acute stress induces a differential increase of 5-HT-moduline (LSAL) tissue content in various rat brain areas. *Brain Res*. 1999;825:152–160.
- Chaouloff F. Serotonin, stress and corticoids. *J Psychopharmacol*. 2000;14:139–151.
- Tafet GE, Toister-Achituv M, Shinitzky M. Enhancement of serotonin uptake by cortisol: a possible link between stress and depression. *Cogn Affect Behav Neurosci*. 2001;1:96–104.
- Hirvonen J, Nägren K, Kajander J, Hietala J. Measurement of cortical dopamine D1 receptor binding with [¹¹C]SCH 23390: a test-retest analysis. *J Cereb Blood Flow Metab*. 2001;21:1146–1150.
- Parsey RV, Slifstein M, Hwang D-R, et al. Validation and reproducibility of measurement of 5-HT_{1A} receptor parameters with [carbonyl-¹¹C]WAY-100635 in humans: comparison of arterial and reference tissue input functions. *J Cereb Blood Flow Metab*. 2000;20:1111–1133.
- Vilkman H, Kajander J, Nägren K, Oikonen V, Syvälahti E, Hietala J. Measurement of extrastriatal D₂-like receptor binding with [¹¹C]FLB 457: a test-retest analysis. *Eur J Nucl Med*. 2000;27:1666–1673.
- Frankle WG, Slifstein M, Hwang DR, et al. Reproducibility of derivation of serotonin transporter parameters with [¹¹C]DASB in healthy humans: comparison of methods [abstract] *J Nucl Med*. 2004;45(suppl):68P.